

# We are IntechOpen, the world's leading publisher of Open Access books Built by scientists, for scientists

6,900

Open access books available

186,000

International authors and editors

200M

Downloads

Our authors are among the

154

Countries delivered to

TOP 1%

most cited scientists

12.2%

Contributors from top 500 universities



WEB OF SCIENCE™

Selection of our books indexed in the Book Citation Index  
in Web of Science™ Core Collection (BKCI)

Interested in publishing with us?  
Contact [book.department@intechopen.com](mailto:book.department@intechopen.com)

Numbers displayed above are based on latest data collected.  
For more information visit [www.intechopen.com](http://www.intechopen.com)



# Forest Fires and Remote Sensing

Abel Calle and José Luis Casanova  
*University of Valladolid,  
Spain*

## 1. Introduction

The use of remote sensing techniques for the study of forest fires is a subject that started already several years ago and whose possibilities have been increasing as new sensors were incorporated into earth observation international programmes and new goals were reached based on the improved techniques that have been introduced. Three main topics can be distinguished, in which remote sensing provides results that can be applied directly to the subject of forest fires: risk of fire spreading, detection of hot-spots and establishment of fire thermal parameters and, finally, cartography of affected areas. In the last years, other two important topics are getting increasing interest; the first one is the estimation of severity, related to the post-fire phase, and the other one is the atmospheric impact of fire emissions.

With respect to the risk of fires, remote sensing has provided very valuable results in real time, which was the required aim. However, in order to be able to predict the existence of fires, it is necessary to incorporate indicators of very heterogeneous types which sometimes fall out of the field of earth observation studies; indicators related to economy, social and human activities or historical statistics among others, should, for example, be taken into account. That's why remote sensing must be restricted to a very limited aspect which makes it only suitable for the estimation of the spreading risk related to the vegetation dryness and surface temperature values. The main magnitude used as an indicator is the vegetation index, above all, the NDVI (Normalized Difference Vegetation Index). The first results in the estimation of the fire risk, although not in real time, were obtained through analyses by the satellites belonging to NOAA (National Oceanographic and Atmospheric Administration) series, by means of AVHRR (Advanced Very High Resolution Radiometer) sensor. Later on, further indicators coming from the same sensors were incorporated so as to improve the algorithms and include the information relative to meteorological conditions like the surface temperature obtained through satellites. The combination of the NDVI with the surface temperature has given place to a mixed index in which the lineal regression slope in both magnitudes established cells of terrain, presents a good correlation with the vegetation evapotranspiration and water stress (Nemani & Running, 1989). The use of the slope in this relation has been incorporated through different algorithms by different authors in order to establish another risk indicator (Illera *et al.*, 1996); thus, Casanova *et al.*, (1998) introduced it to work in real time within the operation in Mediterranean countries. The possibility of using the spectral information in the middle infrared, in the 1.6  $\mu\text{m}$  region, has given place to the introduction of other indicators related to the fuel's moisture since the vegetation's reflectivity in this wavelength interval is strongly influenced by the water contained in it.

Hunt & Rock (1989) suggested a new vegetation index similar in the equation to the NDVI but including the reflectance in the near infrared and the reflectance in the 1.6  $\mu\text{m}$  region, an index indicating the fuel's moisture. At first, this index could only be applied to the Landsat-TM (Thematic Mapper) sensor for the creation of fuel maps (Chuvieco *et al.*, 2002). Today, it can be used in real time on the AVHRR and MODIS (Moderate Resolution Imaging Spectroradiometer) sensors to be incorporated to the risk maps as a new indicator.

The detection of hot spots and, together with it, the establishment of fire parameters, is the most complex task of the ones presented here, due to the orbital configuration of the current spacecrafts. The methodologies are very clear from the point of view of physics, but the restrictions of the current sensors introduce difficulties in order to get quality results. By detection, it is understood the task of determining the location of a hot spot independently of its size. By monitoring, it is understood the establishment of the most important fire parameters with a view to obtain relevant information on this phenomenon. Among these parameters are the fire's temperature, the area taken by the fire, the energy intensity and, when the sensor's capacity allows it, the establishment of the advancing fire line. In order to place this subject of study in its appropriate context, it must be pointed out that fire detection with an aim to create alarms that facilitate a rapid extinction is a necessity that hasn't been fully resolved yet. Despite its limitations the NOAA-AVHRR sensor has been the most important for fire detection and has provided a benchmark for subsequent sensors. An excellent revision of the algorithms used on AVHRR can be found in Li *et al* (2001). The case of the European sensor (A)ATSR (Advanced Along Track Scanning Radiometer) and the World Fire Atlas from 1997 published by the ESA with the ERS-1 and ERS-2 (European Remote Sensing Satellite) satellites data (Arino & Rosaz, 1999) has been used to demonstrate its suitability to fire detection and assessment of vegetation fire emissions. The appearance of the MODIS sensor heralded a significant step forward in the observation of forest fires (Giglio *et al.*, 2003) and, at this moment, the MODIS fire product is a consolidated product and a reference for global Earth observation. Fire product has been identified as an important input for global change analysis; however, although the radiometric availability is satisfactory, the main problem is the time resolution to operate in real time. Detection of high temperature events through geostationary satellites has been taken into account with the different perspective. The improvements introduced in the sensors have allowed us to use geostationary satellites beyond their meteorological capabilities, adapting them to Earth observation; this is the response to the need for series of stable fire activity observations for the analysis of global change, changes in land use and risk monitoring. The GOES (Geostationary Operational Environmental Satellite) has been the worldwide reference for fire monitoring through geostationary platforms. Since 2000, the Geostationary Wildfire Automated Biomass Burning Algorithm (WF\_ABBA) has been generating products for the western hemisphere in real-time with a time resolution of 30 minutes and this detection system has been operational within the NOAA NESDIS programme since 2002. The GOES-East and GOES-West spacecrafts are located in the Equator, providing diurnal coverage of North, Central and South America and data based on fire and smoke detection. The results provided by the GOES programme have been the starting point of a global geostationary system for fire monitoring, initially comprising four geostationary satellites that were already operational: two GOES platforms, from the USA, the European MSG (Meteosat Second Generation) and the Japanese MTSAT (Multifunctional Transport Satellite, covering Southeast Asia and several parts of India as observation regions. The minimum fire

detection sizes of GOES, MSG and MTSAT, with time resolution less than 30 minutes has allowed the international community to think in a global observation network in real time. The implementation of this network is the aim of the Global Observations of Forest Cover and Land Cover Dynamics (GOFC/GOLD) FIRE Mapping and Monitoring program, internationally focussing on decision-taking concerning research into Global Change. The GOFC/GOLD FIRE program and the Committee on Earth Observation Satellites (CEOS) Land Product validation held a workshop dedicated to the applications of the geostationary satellites for forest fire monitoring (Prins *et al.*, 2004).

The cartography of areas affected by fires is a subject that has been dealt with in depth. Remote sensing has proved to be very useful in the study of forest fires cartography and severity since the time resolution does not prevent the subsequent evaluation of the consequences. Different radiometric procedures have been used based on the application of fixed thresholds to the NDVI in the case of low spatial resolution; the results are satisfactory but the difficulty of these procedures lies in the search of a fixed threshold value, because what seems quite probable is the dependence of the threshold values according to the area analysed and the time of the year in which the study is carried out. Methodologies based on neural networks (Al-Rawi *et al.*, 2001) have also been applied although they have the difficulty of training the neural net so that the final results will depend on the variability of the statistical sample used in the preparation of the neural net. The multi-temporal use of the NDVI for the radiometric analysis and the establishment of thresholds on the NDVI through a spatial contextual analysis is a procedure has been used for low spatial resolution. In the case of high spatial resolution, several procedures have been suggested using many different methodologies to be applied to the TM sensor, on board of Landsat satellites being one of the most frequent the spectral classification. However, an important problem is that it requires the distribution of data probability; another disadvantage is that in order to obtain higher quality results a supervised classification of the zones must be carried out, requiring interaction by user. Within the automatic methodologies, the lineal transformations have shown a great capacity for the obtaining of results. Thus, the application of the Principal Components to the reflectance bands obtains almost immediate cartographic results, since they can be analysed visually through a RGB (Red Green Blue) composite of the output components. An issue linked to the fire cartography is the estimation of severity. Each summer large fires affect to the Mediterranean Europe due to changes in traditional land use patterns which have led to an unusual accumulation of forest fuels, notably increasing fire risk and fire severity. According with Roldán-Zamarrón *et al.* (2006), there is interest in finding a quick and affordable methodology for obtaining fire severity maps that can be made available only a few days after the fire, as this information could prove very valuable in the early stages of rehabilitation planning for large fires. These maps should be based on independent data sources, such as remote sensing, employ automatic or semiautomatic methods, and produce results of an acceptable reliability. Remote sensing techniques are a useful tool in order to generate maps showing different degrees of damage affecting vegetation after a large wildfire in an effective manner. Objective of these severity maps is to locate priority intervention areas and plan forest restoration works.

## 2. Fires and climate

Following the GCOS (Global Climate Observing System) document "Systematic Observation Requirements for Satellite-based products for Climate", and ESA Climate

Initiative, the emissions of greenhouse gases (GHGs) and aerosols from fires are important climate forcing factors, contributing on average between 25-35% of total CO<sub>2</sub> emissions to the atmosphere, as well as CO, methane and aerosols. Hence, estimates of GHG emissions due to fire are essential for realistic modelling of climate and its critical component, the global carbon cycle. Fires caused deliberately for land clearance (agriculture and ranching) or accidentally (lightning strikes, human error) are a major factor in land-cover changes, and hence affect fluxes of energy and water to the atmosphere. Burnt area, as derived from satellites, is considered as the primary variable that requires climate-standard continuity. It can be combined with information on burn efficiency and available fuel load to estimate emissions of trace gases and aerosols. Measurements of burnt area can be used as a direct input to climate and carbon cycle models, or, when long time series of data are available, to parameterize climate-driven models for burnt area. Burnt area, combined with other information (burn efficiency and available fuel load) provides estimates of emissions of trace gases and aerosols. Measurements of burnt area can be used as a direct input to climate and carbon-cycle models, or, when long time series of data are available, to parameterise climate-driven models for burnt area (fire is dealt with in many climate and biosphere models using the latter approach). Fire-induced emissions are a significant terrestrial source of GHGs, with large spatial and interannual variability. Detection of active fires serves as part of the validation process for burnt area (i.e., is the burnt area associated with previous observations of active fire). Detection of active fires provides an indicator of seasonal, regional and interannual variability in fire frequency and shifts in geographic location and timing of fire events. Strong empirical relations exist between the FRP (Fire Radiative Power) and rates of combustion; so, the use of multiple FRP observations to integrate over the lifetime of the fire provides an estimate of the total CO<sub>2</sub> emitted. FRP provides a means to derive a CO<sub>2</sub> emissions estimate from remotely-sensed observations without relying on difficult-to-acquire ancillary data on fuel load and combustion completeness factors.

### 3. Fire detection

#### 3.1 Physic principle of fire detection

As is to be expected, the process of the detection of hot spots is based on the use of bands in the middle and thermal infrared spectrum. There are three laws of Physics that govern the detection process: law of Plank, Wien's displacement law and Stefan-Boltzmann's law. The radiance emission corresponding to a body with a temperature of 300 K, as can be the Earth's mean temperature, will have a maximum value close to 10  $\mu\text{m}$ , and a spectral band situated in this one would receive a very strong signal. For a temperature of 800 K, the maximum value will have displaced to wavelengths close to 3.6  $\mu\text{m}$  and whereas the signal here would be very intense, it wouldn't be nearly as intense in higher wavelengths. The fire detection is based precisely on this inversion, which is possible to detect with thermal bands situated in the spectral regions of 11-12  $\mu\text{m}$  and 3-4  $\mu\text{m}$ . Figure 1, shows this physic principle graphically. The location of two generic bands, in the middle and thermal infrared, are also shown. It's clear that at a temperature of 300K, the radiance received in MIR (Middle InfraRed) is lower than the one received in TIR (Thermal InfraRed). However, at 500 K, this behaviour has inverted and now the radiance is higher in MIR.

The basic principle followed for the location of the spectral bands in a sensor, is described through two questions; first: what I want to see? And second: where the atmosphere allows

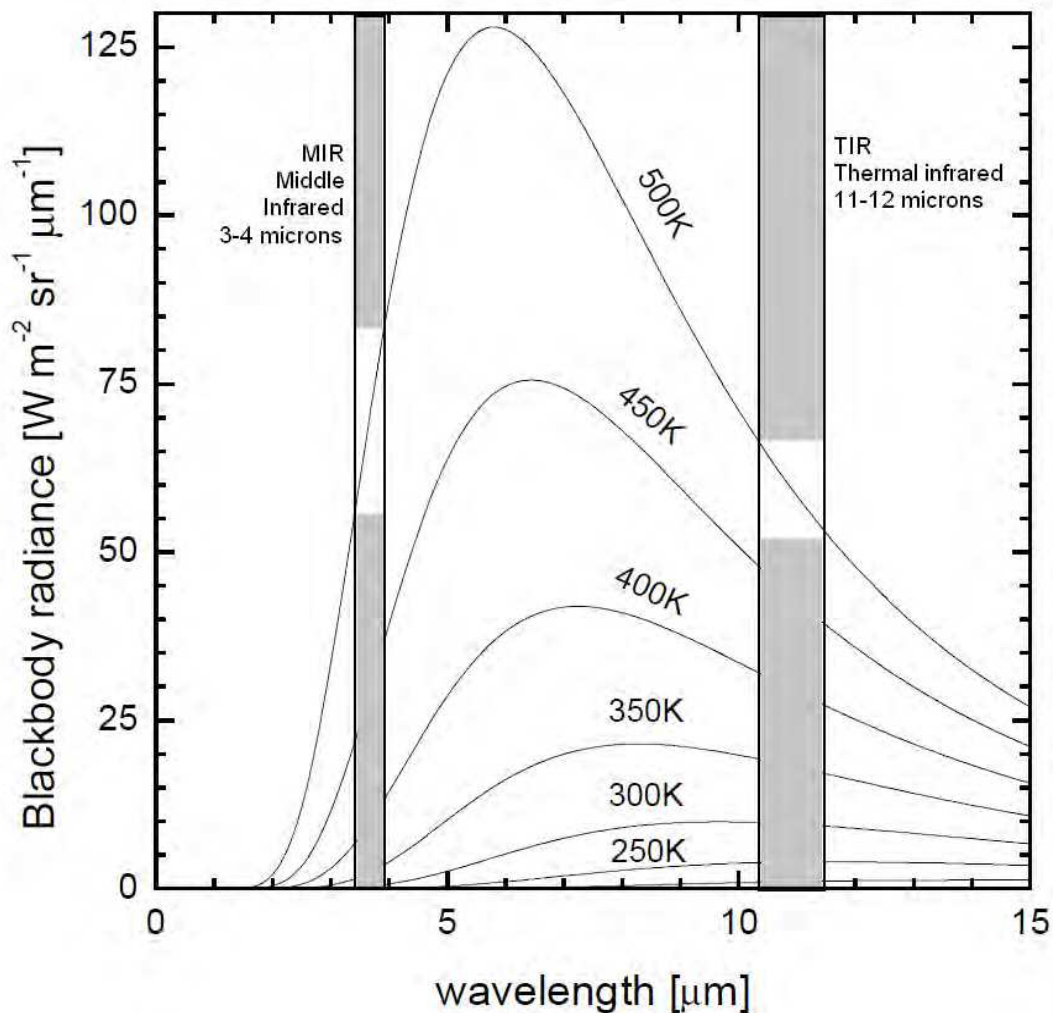


Fig. 1. Law of Planck, showing blackbody emission for different temperatures values of source, and location of MIR and TIR spectral bands (adapted from Li *et al.*, 2001).

me to do? Fortunately, atmospheric absorption is selective in several spectral bands; the water vapour absorption is very strong below  $3.4 \mu\text{m}$  but there is an atmospheric window in the interval  $[3.5-4.2 \mu\text{m}]$ ; so, the MIR bands must be located preventing the absorption of water vapour in the  $3-4 \mu\text{m}$  region. In the case of TIR region, there is a strong absorption band centred at  $9.6 \mu\text{m}$ , due to ozone, but there is an atmospheric window in the interval  $[10-12 \mu\text{m}]$ , with a weak effect of water vapour; it's easy to remove this effect by means of two spectral bands located in this window (split-window technique, Price 1984).

A technical problem to take into account is that the radiance obtained by the sensor, coming from a concrete pixel in which there is a fire, does not only depend on the fire's temperature and, as it is logical, on the temperature of the surrounding surface, but also on the location of the fire inside the pixel since, at the end, the sensor's PSF (Point Spread Function) will determine the filtering that is carried out on the original image. In any case, to obtain a positive detection from an active fire is easy. The main problem to detect fires is to obtain a positive detection when the fire does not exist; that is: a false alarm. The false detections, in the  $4 \mu\text{m}$  region, are due to radiance not only is coming from the emission, but there also exists a component due to the effect of reflection. That's why we can find ourselves in

situations in which a high radiance signal does not necessarily correspond to a high-temperature pixel, except in the case of night observation, when the reflection component, evidently, does not exist. As is to be expected, the radiance that gets to the sensor in that part of the spectrum where the reflection and the emission effects superimpose, as is the 4  $\mu\text{m}$  case. The value of the reflected component  $L_{\text{reflection}}$  is  $\frac{\alpha E_0 \cos(\theta_{\text{sun}})}{\pi}$ , with  $\theta_{\text{sun}}$  being the

sun's zenith angle,  $E_0$  the extraterrestrial sun's irradiance in that spectral band and  $\alpha$  the spectral reflectance (the atmospheric effect are not included). The emission component,  $L_{\text{emission}}$  is  $(1 - \alpha) \cdot B(\lambda, T_{\text{surface}})$ , in which  $B(\lambda, T)$  is the function of Planck,  $\lambda$  the wavelength in that spectral band and  $T_{\text{surface}}$  the surface temperature observed by the sensor. Note that  $\varepsilon = (1 - \alpha)$  and  $\alpha = (1 - \varepsilon)$ , with  $\varepsilon$  the emissivity. If a surface has a high value of reflectance in the MIR region, radiance coming from source is high and brightness temperature will be higher than surface temperature in several Kelvin. As an example, it can be observed that for a reflectance value of 20% and a sun's zenith angle of 30° the brightness temperature can increase more than 20 K higher due to reflectance effect. When the contribution of the reflection component is very marked and as a consequence the radiance increases in the middle infrared band, a pixel appears with an apparent high temperature that can be mistaken with a hot spot, producing a false alarm. These situations are more frequent in the highest spatial resolution sensors and when high reflectance surfaces coincide with sun-satellite geometrical situations close to specular reflection conditions. This is the case of small water surfaces, for example, and it is called *sun glint*. It must be pointed out that the problem of the appearance of false alarms is more difficult to solve than the detection itself due to the difficulty in separating both effects. Finally, it must be mentioned that clouds are also an important source of false alarms due to the sun's reflection. Their reflectance is high and they cause a strong signal in the MIR spectral band in situations of very high sun zenith angles.

### 3.2 Fire detection using heliosynchronous platforms

Not only was the NOAA-AVHRR sensor the first one to provide results, but it has also been a research platform in the development of hot-spot detection algorithms. This has been possible thanks to its high time resolution (among the polar heliosynchronous sensors) and to which the physic principles of detection mentioned above can be applied. It must be pointed out, however, that the AVHRR sensor has important limitations. The most important of these is the low saturation level, 320-331 K (Robinson, 1991), of the main band involved in the detection, the 3.7 $\mu\text{m}$  band. This limit is so low that a fire with a temperature of 1000 K on a non-reflective surface of 300K only needs a 13x 13 m<sup>2</sup> surface to reach the pixel's saturation. This important drawback makes the sensor suitable for the detection of hot-spots but in most cases, it makes it unsuitable for the analysis at a sub-pixel level. In spite of its limitations it is unavoidable to use this sensor as a comparative reference for subsequent, more operative sensors such as MODIS (Ichoku *et al.*, 2003). The detection has been developed through different algorithms that can be schematically classified into algorithms based on fixed thresholds and contextual algorithms, whose parameters have been adapted to the different zones of study. Both types of algorithms have advantages and disadvantages and their application will depend on the type of sensors to which they are going to be applied. The detection algorithms based on fixed thresholds, also called multi-

channel, are based on the establishment of minimum temperature values in different spectral bands from which the detection is established. The most common scheme is to consider that a pixel is affected by a fire when the following conditions are fulfilled simultaneously:

$$T_{MIR} > V_{MIR} ; T_{MIR} - T_{TIR} > V_{DIF} ; T_{TIR} > V_{TIR} ; R_{NIR} < V_{NIR} \quad (1)$$

where  $T_{MIR}$  and  $T_{TIR}$  refer to the brightness temperature in the spectral bands of the 3.7  $\mu\text{m}$  and 11  $\mu\text{m}$  regions respectively, and  $V$  is the adopted threshold. In the former test, the first two conditions are the ones that carry out the detection of hot-spots strictly speaking according to the physic principles previously stated. The  $T_{MIR}$  test is for fire detection and the  $T_{MIR}-T_{TIR}$  test is to carry out the differentiation between the fire, which has high values in the MIR, and the hot surfaces which have high values both in the MIR and TIR. The  $T_{TIR}$  test is a cloud filter to apply the test to images in which the cloud cover has not been removed through other procedures. The  $R_{NIR}$  test is to filter the reflectance in sun-glint situations that are responsible for the appearance of false alarms. The threshold values established are varied. They depend on the algorithm and, above all, on the geographic area due to the influence of the background temperature. Thus, normally low surface temperature values use lower MIR threshold values without the appearance of false alarms. Two examples of this type of algorithms, operating on NOAA-AVHRR, are the used by the CCRS (Canadian Centre of Remote Sensing) (Li *et al.*, 2000) and the ESA (European Space Agency) (Arino and Mellinote, 1998). The disadvantage of the algorithms based on fixed thresholds is that the values established depend on the zone of study and their environmental temperatures. In order to avoid this dependence, contextual algorithms can be used. They are based on the obtaining of threshold values carrying out a statistical analysis of the environment. The basic scheme is summarised in the following test:

$$T_{MIR} > \mu_{MIR} + f \cdot \sigma_{MIR} ; T_{MIR} - T_{TIR} > \mu_{DIF} + f \cdot \sigma_{DIF} ; R_{NIR} < \mu_{NIR} - f \cdot \sigma_{NIR} \quad (2)$$

where  $\mu$  and  $\sigma$  are the mean values and the standard deviation in the environment of the pixel analysed and  $f$  is a factor that has to be established. The environment is analysed in a matrix with a size of  $N \times N$  pixels, being  $N$  an odd value depending on the sensor to which it is applied. Two examples are the IGBP (International Geosphere and Biosphere Programme) algorithm (Justice & Malingreau, 1993), and an adaptation of the current algorithm on MODIS (Kaufman *et al.*, 1998). Contextual algorithms have the advantage of making the detection process independent from the season and the zone analysed, since the thresholds are obtained by means of a statistical analysis of the environment. However, they have a serious drawback when they are applied to images in which the clouds have not been filtered since cloud edges cause false alarms. A variant to the basic contextual algorithm exposed is the one suggested by Lasaponara *et al.* (1998), in which the mean statistical parameters and the standard deviation are determined by using not just the spatial environment but also the temporal one, extending the matrix of analysis to the images of previous days, looking for the changes in the brightness temperature not only in a spatial scale but in a temporal interval too.

The launch of the MODIS sensor in 1999 on the Terra platform and in 2002 on Aqua with 36 different-spatial-resolution spectral bands has provided much more reliable results in detection. This sensors includes two spectral bands in the 4  $\mu\text{m}$  spectral zone with saturation

values very high to the MIR AVHRR band and the applied algorithm uses a large number of bands to consolidate the results. Another important characteristic of MODIS is an excellent radiometric resolution of 12 bits (instead AVHRR sensor with 10 bits) very interesting to fire monitoring. The original algorithm has been improved (Giglio *et al.*, 2003) and it carries out three test phases: cloud cover filtering, detection and consolidation test. The cloud-and-water-filtering phase uses three spectral bands: the reflectances in bands 1 and 2 with a spatial resolution of 250 meters, centred in 0.65  $\mu\text{m}$  and 0.86  $\mu\text{m}$ , respectively, and the temperature in the band of 12  $\mu\text{m}$ ,  $T_{12}$ . Thus, the pixels fulfilling any of the three following conditions will be rejected: having a  $T_{12}$  value lower than 265 K or a sum of reflectances higher than 0.9 or  $T_{12}$  lower than 285 K and sum of reflectances higher than 0.7 simultaneously. First, the detection phase establishes the potential pixels that must be analysed according to the criteria used by AVHRR with fixed thresholds, analysing the temperature in band 21, around 4  $\mu\text{m}$ , establishing a threshold of 310 K and the difference of this band with band 31, around 11  $\mu\text{m}$ , with a threshold difference of 10 K. Later, the identification of fire pixels, among the potential ones, is carried out through two procedures: first, an absolute test for the ones that have a  $T_{4\mu\text{m}}$  value higher than 360 K during the day and 320 K at night. Secondly, an alternative test which carries out a characterisation of the environment's temperature through a contextual analysis on the pixels that were not considered potential and with a variable window until a significant number of points is obtained. This contextual analysis is similar to the one used by the AVHRR algorithms, but it follows additional steps to eradicate false alarms and it differentiates between day and night pixels. The methodology considers three different sources of false alarms: the first one is the possibility of sun-glint, which is solved through a geometrical analysis with the sun-pixel-satellite directions in order to reject situations of specular reflection; the second one are hot desert pixels and the third one the coast lines. The two latter are solved through the establishment of temperature and reflectance thresholds simultaneously. Finally, the consolidation phase establishes a statistical analysis to obtain well-confirmed pixels affected by a fire. This is due to the fact that the spatial resolution of MODIS in the thermal is 2 km, with step of 1km. This may cause that the same fire, located in a zone where two pixels are superimposed can be revealed by both of them. The consolidation test is carried out on the pixels adjacent to the one which is being analysed. More details about the algorithm can be seen in (Giglio *et al.*, 2003). It must be pointed out that MODIS has two bands in the MIR region used in detection: bands 21 and 22, both centred in the 3.9  $\mu\text{m}$ . The difference is that the saturation level for the first one is 500K whereas for the second one it is 331. However, band 22 has less noise and a smaller error in the calibration. That's why, if the pixel is not saturated, the algorithm uses band 22. Otherwise, band 21 is used.

In spite of the tools we have shown for fire detection, it must be said that their results have not been brought into operation due to the lack of continuity in the monitoring of heliosynchronous satellites. Several monitoring programmes have been designed based on the co-ordination of several satellites in different orbital planes in order to increase the number of daily observations on a concrete place. Projects such as FUEGO originally and FUEGOSAT nowadays, are funded by ESA in order to obtain a product that can be put into operation for the monitoring of forest fires. On the other hand, the effectiveness in detection, of the sensors mentioned, could be improved through the design of sensors specially dedicated to fire detection. There was a prototype satellite fulfilling these characteristics and that has provided results to be analysed. It is the BIRD (Bi-spectral Infrared Detection),

designed by the DLR German laboratory, as a sensor prototype, and its detection capacities have been very satisfactory thanks to its design (Briess *et al.*, 2003); the HSRS (Hot Spot Recognition Sensor System), with a visual field of  $19^\circ$  (190 km), a spatial resolution of 370 m and a radiometric resolution of 14 bits. Apart from the new spatial resolution in the thermal and its excellent radiometric resolution, this sensor is able to establish a dynamic rank of calibration that is completed with two successive expositions of the scene with a short time of integration; this makes it possible to establish a saturation limit close to 1000K, with a temperature resolution in the interval [0.1-0.2 K]. The algorithm includes 5 consecutive tests through which different threshold values of analysis are established: an adaptive test in the MIR to detect potential hot-spots, a threshold in the NIR to reject the sun reflection, which is a source of false alarms during day observations, a threshold adaptive to the MIR/NIR fraction of radiances to reject clouds and other high-reflective objects, a threshold adaptive to the MIR/TIR fraction of radiances to reject hot surfaces and finally, the gathering of pixels that are adjacent to the fire to obtain the fire's temperature and area parameters. It is important to mention that all the adaptive thresholds mentioned are obtained through the contextual spatial analysis. BIRD satellite must be considered as a very low-cost prototype to operate with several units in orbital co-ordination. The fire parameters provided by BIRD have been able to locate the flaming front very accurately (Wooster *et al.*, 2003).

### 3.3 Fire detection using geostationary platforms

As we have mentioned in the section "Introduction", the geostationary sensors can improve the fire detection results, due to its very short revisit time, even when spatial resolution is very limited due to location in space of geostationary platforms. Currently, the users international community feels that a real-time global observation network may become a reality by means of geostationary sensors such as GOES, MSG and MTSAT. This is one of the objectives of the Global Observations of Forest Cover and Land Cover Dynamics (GOFC/GOLD) FIRE Mapping and Monitoring program, focussing internationally on decision-taking concerning research into Global Change and its ecological and environmental implications. Major efforts are also being made by ESA-EUMETSAT to increase the use of MSG in environmental observation tasks. SEVIRI (Spinning Enhanced Visible and Infrared Imager) on board MSG platforms is a very interesting example of suitable sensor to perform forest fire monitoring in real time (Calle *et al.*, 2006). Some analyses are shown in the particular case of the geographical latitude of the Mediterranean Europe where, during the last years, detection campaigns and dissemination of results in real time have been carried out. The theoretical analysis of the minimum detectable size, including atmospheric effects and saturation conditions, are especially important to delimit the operational range of this sensor in Mediterranean latitudes, where the effects of forest fires are increasingly devastating each year, both in terms of financial as well as human losses. MSG-SEVIRI is geostationary sensor with a time resolution of 15 minutes; so, the comparison between successive scenes provides reliable results once the difference temperature threshold is established for such an interval. Thus, if a Time Thermal Gradient, TTG, higher to the one considered as normal, is detected, we will have a high temperature event. In order to estimate this gradient let's consider a day's thermal evolution as a sinusoidal curve responding to the form:  $MIR\_Temp = A \cdot \sin(\omega t - \delta) + B$ ;  $\omega = \frac{2\pi}{T}$ ; where T is the day's period in units of 15 minutes ( $T=96$ ), A is semi-daily thermal oscillation and B is

a not relevant coefficient. According to this model, the maximum difference in the MIR standard temperature between two consecutive SEVIRI scenes is  $\pm 1.5\text{K}$  for a diurnal-cycle thermal oscillation of around  $30\text{K}$ , which is typical of summer days in middle latitudes. This estimation agrees with the experimental values found in the analysis of the series of MIR temperature evolution curves selected for different test sites in the Mediterranean Europe, during summer. Like this, the maximum temperature difference found, in absolute values, in the 98.2% of cases was lower than  $2\text{K}$ . The averaged of differences found, only considering the intervals with thermal variability [05:00-11:00 GMT] and [14:00-20:00 GMT], was  $1.2\text{K}$ , with a standard deviation of  $0.5\text{K}$ . So, we have considered appropriate to establish a threshold of  $4\text{K}$  as the temperature increase value to detect the beginning of a fire without providing false alarms. In any case, it must be pointed out that there are two daily periods very well defined: from sunrise to midday, in which the temperature is increasing and where the estimation of  $4\text{K}$  is appropriate, and the second one between midday and sunset, for which a value of  $2\text{-}4\text{K}$  would be enough, being a negative gradient. During night periods detection is easier. In order to estimate minimum fire size detectable by the SEVIRI sensor, simulations have been done by means of MODTRAN radiative transfer code (Berk *et al.*, 1996) by introducing different surface and fire temperatures according to different time thermal gradient values. Radiance observed by sensor was simulated as:  $L_{\text{sensor}} = p \cdot L_{\text{fire}} + (1 - p) \cdot L_{\text{surface}}$

where  $p$  is the surface fraction affected by fire and where two homogeneous phases have been considered: fire and surface;  $L_{\text{fire}}$  and  $L_{\text{surface}}$  are the radiances incoming from fire and surface. Spectral radiance was integrated with  $20\text{ cm}^{-1}$  resolution by means of spectral response function and considering different atmospheric attenuation conditions. Results are shown in figure 2, for a standard atmosphere of middle latitude summer and aerosol depth according to visibility  $23\text{ km}$ . Abscissa axis shows the potential fire temperature and ordinate axis shows the minimum detectable area expressed in ha. Different magnitudes of influence must be analysed separately, being the most important the threshold of TTG considered,  $\frac{\partial T}{\partial t}$ , but geographic latitude of observation too. The figure contains the results for three different values of the gradient:  $4$ ,  $6$  and  $2\text{K}/15_{\text{minutes}}$  and for two locations-type, at  $20^\circ$  and  $50^\circ$  latitude. With respect to the latitude, it must be taken into account that although the pixels's area in the nadir point is  $9\text{ km}^2$ , at latitude of  $20^\circ$  it is  $10\text{ km}^2$  and at  $50^\circ$  it has increased up to  $18\text{ km}^2$ . Thus, for a required gradient of  $4\text{K}/15_{\text{min}}$  and a fire of  $600\text{K}$ , the detectable area at  $20^\circ$  latitude is  $0.5\text{ ha}$ , whereas at  $50^\circ$  latitude it would be  $1\text{ ha}$ . The geographic longitude has not been analysed since it has a very low distortion in the pixels' area. With respect to the thermal gradient,  $4\text{K}/15_{\text{min}}$  is the reference for the analysis carried out in previous paragraphs. The figure shows results for a value  $2\text{K}/15_{\text{min}}$  that can be applied in the descendant period of daily thermal evolution [14.00-20:00], because during this period  $\frac{\partial T}{\partial t} < 0$  is expected and the value  $2\text{K}/15_{\text{min}}$  could be enough. This means that during the evening, fires are more easily detected through this methodology and the fire starting can be established at  $600\text{K}$  with  $0.24\text{ ha}$  at  $20^\circ$  latitude and  $0.48\text{ ha}$  at  $50^\circ$  latitude. As can be seen, the detectable sizes during the day at  $20^\circ$  latitude are similar to the ones in the evening at  $50^\circ$  latitude. Latitude has influence in the variability of the pixel's area and in the atmospheric transmittance, with the cenital angle, which has also been taken into account to obtain results. Results obtained for different atmospheric profiles do not differ too much. Another very important magnitude to be considered is the surface temperature since the considered methodology is presented with continuity throughout the day and night, a

period for which different values are presented. It must be pointed out that lower surface temperatures make the detection considerably easier. Thus, if we go down from 300K to 290K, there is a decrease in the minimum detectable area of around 20-23%. This value is constant for different fire temperatures and also independent from the latitude considered.

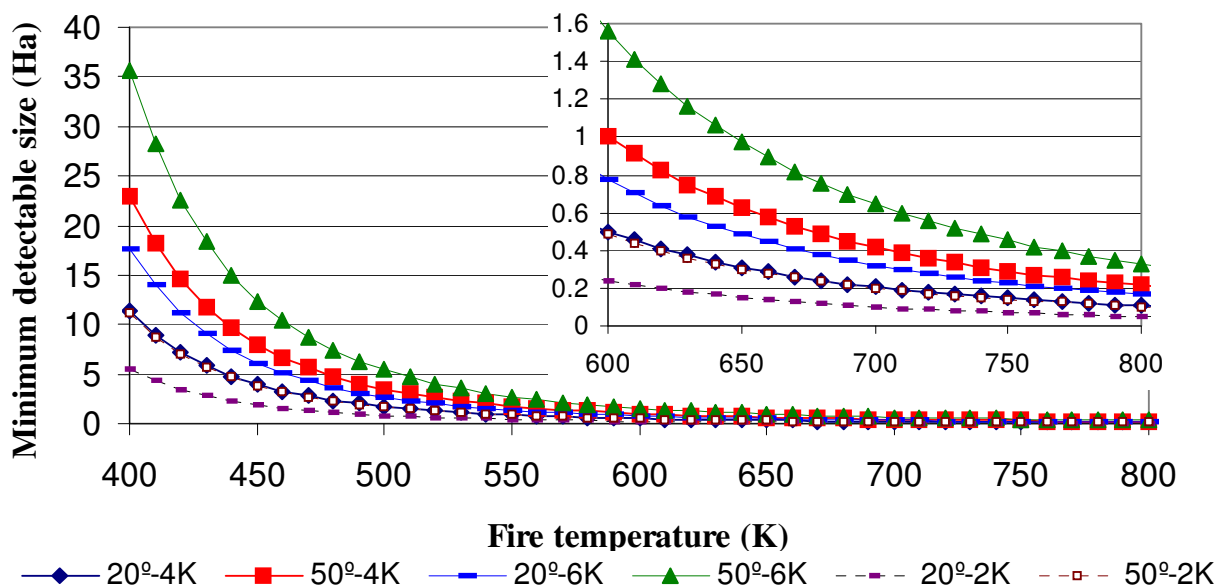


Fig. 2. Minimum size of fire (ha) to be detected by SEVIRI, for different fire temperature and latitude, applying TTG values of 2, 6 and 4K/15\_minutes, taking into account atmospheric attenuation (taken from Calle *et al.*, 2006).

Establishing the outbreak of a fire, as accurately as possible, is crucial to alerting fire-fighting teams as quickly as possible. If the detection process takes into account the comparison with the previous image the delay can be up to 30 minutes in the worst cases. To show some representative results we have analyzed the day on which Spain's worst fire in the previous decades in terms of human losses occurred. This fire, which started between 12:30 and 12:45 on 16th July 2005, spread for over five consecutive days and devastated around 13,000ha. Figure 3 shows the image of the 3.9  $\mu\text{m}$  spectral band corresponding to a few hours after the fire. The visual analysis of the image shows the existence of many fires in Spain and Portugal. Given their importance, two have been highlighted and shown. Number 1 is the fire in Guadalajara (Spain) and number 2, one of the fires that affected the natural park of Lago de Sanabria (Zamora, Spain) during the summer of 2005, whose initial characteristics, as will be seen, differ from the first. In the figure, we have indicated the wind direction in fire #1 from the smoke plume, which is perfectly visible and which will be useful later to analyze the spread of the fire. Below in the same figure are the two thermal evolution diagrams corresponding to these fires. The diagram shows the temperature evolution of band 3.9  $\mu\text{m}$ , in  $^{\circ}\text{C}$ , in the primary axis of the ordinate according to the time of the day, between 06:00 and 16:00 GMT. The secondary axis of the ordinate shows the evolution of the time thermal gradient of the same band, in  $^{\circ}\text{C}/15\text{minutes}$ . If we compare both temperature evolution curves, we can see that they are practically identical on the primary axis up to the moment at which the fire starts, at 12:30 in #1 and at 13:45 in #2 despite being different vegetation covers with different fuel moisture content since they

occur in different climate zones. The analysis of the curve of the time thermal gradient is much more conclusive. The change in the temperature value is  $1.5^{\circ}\text{C}/15_{\text{minutes}}$  in both curves prior to the outbreak of the fire reaching a maximum of 2.3 in #1 and 1.8 in #2, which are exceptional considering the rest of the values. Case #2 was a fire that started with a time thermal gradient of  $4.2^{\circ}\text{C}/15_{\text{minutes}}$  in the first scene at 14:00 GMT, immediately jumping to  $15^{\circ}\text{C}/15_{\text{minutes}}$  in the following scene at 14:15 GMT. It is clear that it began between 13:45 and 14:00 as the figure shows. The case of fire #1 presents a much more abrupt beginning, with a time thermal gradient of  $8^{\circ}\text{C}/15_{\text{minutes}}$  in the first scene at 12:45 GMT. In this case, the fire broke out between 12:30 and 12:45 GMT. Apart from its initial causes, the characteristics of a fire at its onset depend on the combustible material and moisture. In this comparison, it is not surprising that the outbreak was slower in case #2, whose gradient was below #1, as this was a climate zone with higher moisture content.

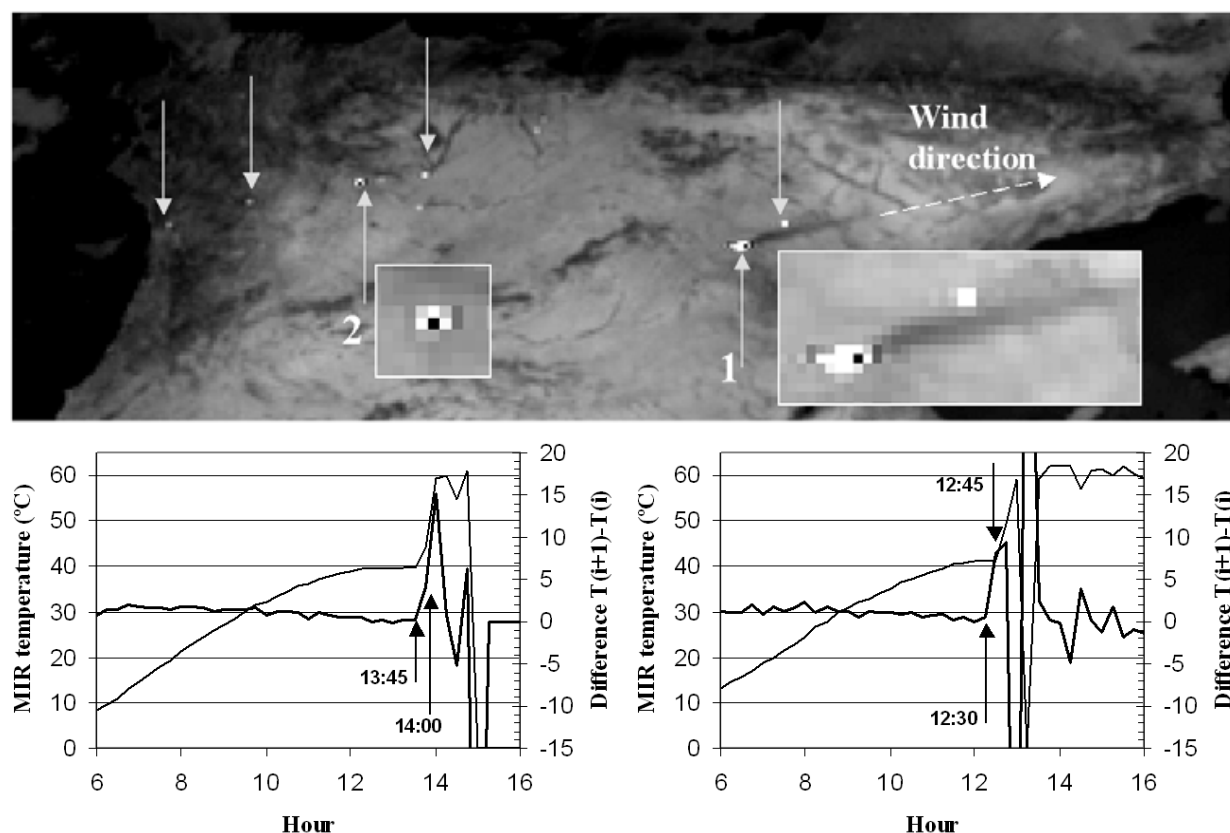


Fig. 3. This figure shows the methodology to detect the start of a fire for two different cases. The upper part of the figure shows the  $3.9 \mu\text{m}$  band, highlighting several fires (validated by MODIS) as well as wind direction. The second part shows the thermal evolution, in the left scale, and the time thermal gradient, in the right scale, in  $^{\circ}\text{C}/15_{\text{minutes}}$ , for the two selected cases. (Calle *et al.*, 2006).

The methodology proposed to detect the beginning of the fire is no longer valid as the fire keeps developing since the temperature differences between the different scenes experiment strong variations. Even the frequent appearance of saturated pixels causes sharp changes that cannot be analysed. Further, for the subsequent monitoring of the fire, a methodology for detecting hot spots (after the starting) is required. Detection methods on other sensors used as a reference are sometimes based on physical models. However, experimental

statistical models have shown better results and are easier to apply as the contextual models operating on AVHRR and MODIS, as we have seen in the paragraph before.

### 3.4 Spatial characterization of fire detection

The pixel dimension is the main parameter that characterises sensors concerning their spatial resolution. However, the radiance quantification and image interpretation need an appropriate analysis to obtain several physical parameters. The review of Cracknell (1998), describes spatial and radiometric considerations regarding the pixel precisely. In order to answer the question “what’s in a pixel?”, title of the mentioned paper, it is firstly necessary to carry out an accurate analysis of the target area that emits the radiance reaching the sensor which, in fact, never coincides exactly with the spatial resolution assigned to it nor with the square shape that it is imagined for the matrix elements of an image. The simplified concept of image as a mosaic of elements is quite far from the reality, something that becomes evident when trying to observe image detail or compare images from different sensors with similar spatial resolution. Moreover, the concept of spatial resolution is often identified with Ground Sampling Distance (GSD), defined as the distance between centres of neighbour pixels, or the use of Instantaneous Geometric Field of View (IGFOV), the geometric size of the image projected by the detector on the ground through the optical system introducing confusion in the sensor’s spatial characterization. Since there are sensors with similar IGFOV but different Modulation Transfer Function (MTF), it is more realistic to define a quantity in the topic of MTF. The concept of Effective Instantaneous Field Of View (EIFOV) introduced by NASA, 1973, is defined as the resolution corresponding to a spatial frequency for which the MTF system is 0.5. The MTF shape in the frequency domain and, consequently, the Point Spread Function (PSF) in the spatial domain has not a special relevance when the surface observed shows a homogeneous distribution of radiance; nevertheless, when there are heterogeneous distribution of radiance inside the pixel, as is frequently the case of forest fires, PSF and deconvolution processes must be considered. In this paragraph, results by using real MTF functions of the SEVIRI sensor, are shown.

On the other hand, many thermal parameters in remote sensing are estimated by solving multi-spectral processes, such as the estimation of the temperature using split-window procedures or the estimation of thermal parameters in hot-spots through Dozier’s method (Dozier, 1981; Matson and Dozier, 1981). In these estimations, it is assumed that the pixels of the bands involved correspond to the same spatial target and contribute with the same sensitivity to the radiance measurement. However, even in the case of a perfect co-registration between bands, this assumption would not be true since each band has a different PSF. This is one of the problems mentioned by Wooster *et al.* 2005, in order to propose a single-channel method to estimate the fire temperature instead of applying a bi-spectral method. In addition, the influence of the PSF has been highlighted as responsible for the differences in the Fire Radiative Power (FRP) when different sensors are compared. Concerning geostationary satellites, MSG is providing operational results in fire detection and biomass burning in Africa (Wooster *et al.*, 2005) and Mediterranean countries (Calle *et al.*, 2006) and Geostationary Operational Environmental Satellites (GOES) are used operationally in South-Central-North-America (Prins and Menzel, 1994). The issue of fire detection is understood in the framework of global geostationary fire monitoring applications and requires evaluating the impact of the MTF’s shape in the estimation of thermal parameters.

In order to estimate the impact of PSF shape on detection suitability, it's interesting to analyze a sensor with low spatial resolution, as SEVIRI sensor onboard of MSG satellite (Calle *et al.*, 2009). Pixel affected by fire appears a typical cross shape when fire is detected, due to PSF effects and overlapping between pixels. Figure 4 shows a three-dimensional graph where the brightness temperature in the  $3.9 \mu\text{m}$  band (vertical axis) is shown versus the fire temperature (left part of figure) and background temperature (right part of figure) and the distance from the pixel centre (PSF impact), where the background temperature is 300 K (left), the fire temperature is 500 K (right) and the one-dimensional burning area is 50m (both cases). Saturation plane is shown in the figures. Note that for low fire temperatures (below 450 K, taking into account that we are talking of flaming and smouldering mixed phases, the PSF impact is not noticeable. However, large differences in brightness temperature are found in hotter fires. In order to explain the importance of a 10 K-difference in the  $3.9 \mu\text{m}$  band, note that if a contextual detection algorithm is applied the detection will be lost when the standard brightness temperature deviation around the pixel is higher than 3 K.

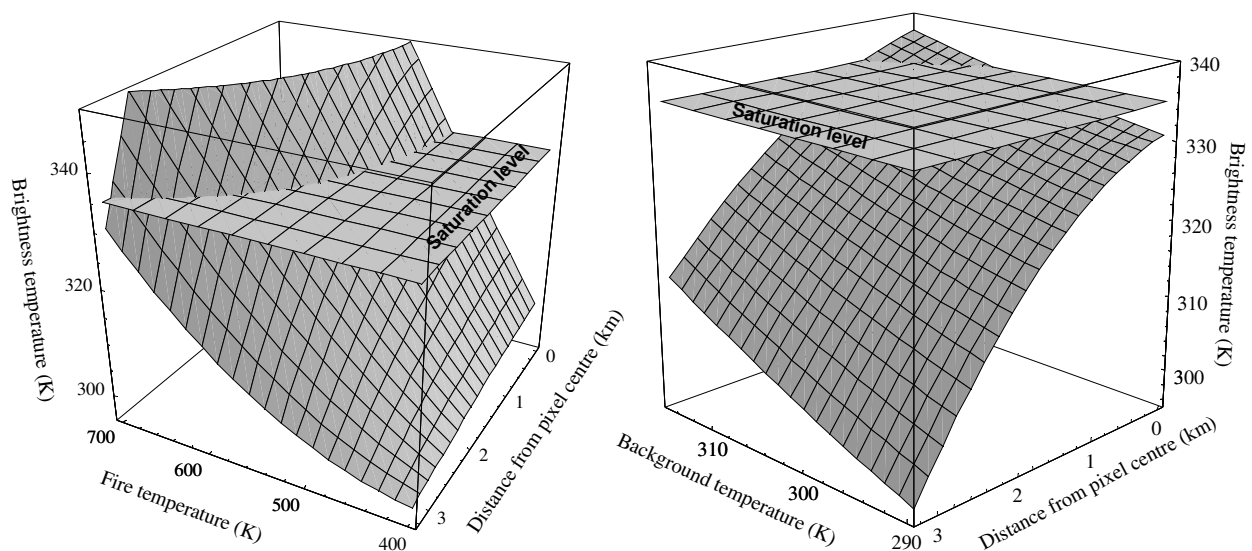


Fig. 4. Left part: Brightness temperature in the  $3.9 \mu\text{m}$  band (vertical axis) versus fire temperature and distance from pixel centre (PSF impact); background temperature 300 K is considered. Right part: Brightness temperature in the  $3.9 \mu\text{m}$  spectral band (vertical axis) versus background temperature and distance from pixel centre (PSF impact). fire temperature of 500 K is considered. One-dimensional burning size of 50 m. (Calle *et al.*, 2009)

#### 4. Fire monitoring

The concept of detection is very clear, but it is not so clear the concept of monitoring. It could be said that monitoring comprises all the aspects related to the knowledge of a fire while it is taking place. Thus, we can talk of the fire temperature, the active area, the fire's energy intensity and the fire's front. However, all these parameters are subject to the technical possibilities of the spatial sensor used, especially the spatial resolution in the thermal spectrum. The main problem with monitoring tasks lies in the necessity of having available the time resolution typical of geostationary satellites in order to be able to know

not just the instant value of the above mentioned parameters, but also their evolution throughout the fire's development. However, these sensors are currently very far from providing detailed results. Next, we will see the type of information we can get according to the capacities of different sensors.

For the knowledge of fire parameters, we need first an analysis at a sub-pixel level through the application of Dozier's methodology (1981). This methodology allows us to establish both the fire temperature and the fraction of the area that is burning simultaneously. This procedure can be applied to any sensor and it is based on the solution of the following system of equations: given a pixel affected by a fire at a temperature  $T_f$  that occupies the fraction of the pixel  $p$ , and it is surrounded by a surface at a temperature  $T_{surf}$ , then the radiances detected in the MIR and TIR bands will be given by the expressions:

$$\begin{cases} L_{MIR} = pB(\lambda_{MIR}, T_f) + (1-p)B(\lambda_{MIR}, T_{surf}) \\ L_{TIR} = pB(\lambda_{TIR}, T_f) + (1-p)B(\lambda_{TIR}, T_{surf}) \end{cases} \quad 0 < p < 1 \quad (3)$$

where  $L_{MIR}$  and  $L_{TIR}$  are the radiances observed by the sensor in the spectral regions of  $3.7\mu\text{m}$  and  $11\mu\text{m}$  respectively and  $B(\lambda, T)$  is the function of Planck. This system of equations provides the fire temperature value and the fraction of the pixel that is burning.

Before analysing some approximations taken in this methodology, we must point out two very important restrictions concerning its operating capacity. In the first place, it must be said that the equations are based on the establishment of the radiance emitted by the thermal spectrum. The  $11\mu\text{m}$  region has no other nature, but the radiance observed in the MIR region has a reflection component that has been analysed in the false alarms section. That's why, the application of these equations to diurnal images should include an additional solar term. Otherwise, they would only be valid for night images. On the other hand, in order to obtain reliable results, it is necessary to avoid saturation as much as possible.

Dozier's system of equations is very simple to understand although many of the approximations it takes are not realistic and should be analysed. In the first place, the pixel observed is divided into two parts, fire and surface, those are considered homogenous, but this is not the case, especially because of the surface's heterogeneity. On the other hand, the atmospheric effects have been neglected in this scheme. The most serious approximation with respect to the error magnitude is probably found in the establishment of a surface temperature value. Dozier suggested for this value the mean value of the pixels surrounding the fire but not affected by it. It must be highlighted that the results obtained depend to a great extent on this parameter. Simulations carried out on a real fire changing the surface temperature value (Calle *et al.*, 2005) show that the error in the surface temperature affects the fire temperature with a value multiplied by 10. Finally, another approximation taken is not to include in the equations the emissivity of the radiance received by the sensor. Although it is true that the fire performance is very similar to that of a blackbody, the same does not happen with the non-affected surface, which seems to have variable values. The deduction of the emissivity is justified in the fact that the zones observed for fire purposes are always forest zones and the emissivity values in this kind of environment are comprised in the interval [0.983-0.995] for the TIR band. A more realistic scheme derived from Dozier's

methodology is the one suggested by Giglio & Kendall (2001). This scheme modifies the former one by including terms of emissivity, atmospheric effects and sun reflection in the radiance equation of the MIR band. The following are the modified equations of Dozier:

$$\begin{cases} L_{MIR} = \tau_{MIR} p B(\lambda_{MIR}, T_f) + (1-p)L_{surf,MIR} + pL_{atm,MIR} \\ L_{TIR} = \tau_{TIR} p B(\lambda_{TIR}, T_f) + (1-p)L_{surf,TIR} + pL_{atm,TIR} \end{cases} \quad 0 < p < 1 \quad (4)$$

where  $L_{atm,MIR}$  and  $L_{atm,TIR}$  are the radiances emitted by the atmosphere to the sensor in the MIR and TIR bands respectively. These terms are worthless with respect to the radiances emitted by the surface,  $L_{surf,MIR}$  and  $L_{surf,TIR}$ , and can be disregarded.  $\tau$  is the atmosphere's spectral transmittance. The difference in these equations with respect to the original ones lies in the intervention of the radiances of the surrounding pixels instead of the temperature and finally, although they are taken into account, the surface's emissivity and temperature are not usually known explicitly. The techniques mentioned for the obtaining of fire parameters imply some difficulties related to the errors that are made. In the first place, they are not analytic equations so that their solution must be found by means of numerical calculation techniques. However, it must be said that their solution comes, in the end, from a convergent system. Other important sources of errors have their origin in different magnitudes that have been analysed by Giglio & Kendall (2001) and that will be mentioned here next.

First, a source of error in the results is the error in the calculation of the surface's radiance introduced in the equations. The values for the fire temperature and size are more sensitive to errors in the radiance of  $11.0\mu\text{m}$  than in the  $3.7\mu\text{m}$ . At low temperatures, this is not a big error, but, with a high fire temperature, the error increases noticeably both in the fraction of the pixel affected and in the fire temperature itself. Another source of error to consider is the one corresponding to the atmospheric transmittance. However, in this case, the errors made in the temperature and fraction of the pixel affected, are compensated in the MIR and TIR bands as long as such errors are caused by either an underestimation or an overestimation in both cases. Otherwise, the errors in the results will add up. Thus, an overestimation in the MIR transmittance overestimates the temperature calculated whereas an overestimation in the TIR transmittance produces the opposite effect. A third source of error in the calculations is due to the instrument's noise, although in this case it introduces an accidental systematic error. Finally, the omission of the atmospheric radiance that reaches the sensor is less important than the causes considered formerly, so that in no case does the temperature go over 1.5K or the area over 2%. A very interesting aspect in the theory developed is the one that refers to the fire's emissivity. A fire has always been considered as a blackbody. In fact, and strictly speaking, this is only true when the length of the flame seen from the sensor is larger than 6 metres (Langaas, 1995). This would make us reconsider this aspect in the case of smaller fires so that in these cases we should consider the fire as a grey body. In these cases that separate from the characteristics of a blackbody, the errors made for considering that the fire has an emissivity one, result in an underestimation of both the fire temperature and the fire area, and they are independent from the fraction of the pixel that is affected and the fire temperature. In spite of all the methodology developed, it is important to point out that a forest fire is, in reality, a very complex phenomenon in which different series of phenomena overlap. In this situation, we could ask ourselves what the parameter

we call “fire temperature” is exactly and what the “burning area” is. The model presented is a simplification from the real phenomenon since, up until now, only two phases have been differentiated: the fire flame and the surface. In reality, it should at least be considered the middle phase corresponding to the smouldering. However, it must be taken into account that the introduction of further terms in the model would imply having more spectral bands available in order to obtain more equations and to be able to find all the unknown quantities. We are going to consider this aspect so as to reach some conclusions in relation with the appropriate spectral information. Kaufman *et al.*, (1998) introduced a modification in Dozier’s methodology in order to include the flame phase, which is hotter, and the smouldering phase, which is in the middle between the surface and the flame. Thus, if we call  $p_f$  and  $p_s$  to the fractions of the pixel corresponding to the flame and the smouldering respectively, the bi-spectral equations will be as follows:

$$\begin{cases} L_{MIR} = \tau_{MIR} [p_f B(\lambda_{MIR}, T_f) + p_s B(\lambda_{MIR}, T_s)] + (1-p)L_{surf, MIR} + pL_{atm, MIR} \\ L_{TIR} = \tau_{TIR} [p_f B(\lambda_{TIR}, T_f) + p_s B(\lambda_{TIR}, T_s)] + (1-p)L_{surf, TIR} + pL_{atm, TIR} \end{cases} \quad 0 < p < 1 \quad (5)$$

so that  $p_f + p_s = p$  is fulfilled. The analysis and discussion will be done through the flaming ratio function,  $f$ , defined as  $f = \frac{p_f}{(p_f + p_s)}$ . This relation is related to the importance that

the flame phase has in the fire observed. Since in order to obtain more detailed information, more observation wavelengths are needed, Giglio & Justice (2003) established the errors found according to the pair of wavelengths used to solve the bi-spectral equations so as to establish the most appropriate pair for this purpose, always considering the atmospheric windows for the observation. These authors carried out simulations with combinations of wavelengths in the interval [1.6, 3.8  $\mu\text{m}$ ] for the MIR region and in the interval [2.4, 11  $\mu\text{m}$ ] for the TIR region so that  $\lambda_{TIR}$  was always higher than  $\lambda_{MIR}$ . The most relevant conclusions of this analysis were that the shortest pairs of wavelengths provided higher fire temperatures and smaller areas since the decrease in  $\lambda$  implies a major importance in the flame phase whereas an increase in  $\lambda$  gives more importance to the smouldering phase. It is also interesting that the results of the pair [3.8, 11.0  $\mu\text{m}$ ] and of the pair [3.8, 8.5  $\mu\text{m}$ ] are practically identical, with differences inferior to 5K for the temperature and 5% for the area. This means that the spectral difference in the AVHRR and MODIS sensors, which correspond to the first pair, and in BIRD, which corresponds to the second, are not significant.

MODIS has several bands situated in the spectral region of 4 $\mu\text{m}$ . One of them has a saturation value of 500K (band 21), which makes this sensor especially suitable for the establishment of fire parameters since it is difficult to find saturated pixels. It must be taken into account that it is very rare when this monitoring phase can be applied to the AVHRR sensor since, although the detection is possible, band 3 is very frequently saturated. Likewise, BIRD prototype is especially suitable for the obtaining of parameters and the establishment of the FRP (Free Radiative Power) (Kaufman and Justice, 1998). By definition, the FRE (Fire Radiative Energy) is basically the portion of chemical energy released during the burning of the vegetation and emitted as radiation during the combustion process. These parameters are comprised within the goal of fire analysis and the FRP is precisely the most important one because it contains information both on the emissions produced in the

atmosphere by these events (Kaufman *et al.*, 1996) and on the fire's destructive power. These authors have suggested that the quantification of the radiated energy during the combustion process in the fire could supply a measurement related to the quantity of vegetation consumed per unit of time. Consequently, it would provide a measurement of the emissions produced during fires and, therefore, it would provide valuable support information to the processes of climate change obtained through remote-sensing. In spite of being a qualitative measurement of great value, we must take into account that the combustion phase is a mixture of physic processes through which the fire's energy is distributed, apart from the radiation phase, as is the case of the air mass convection above the fire and the conduction towards the interior of the earth.

For the MODIS sensor case, Kaufman & Justice (1998), have suggested an empiric expression in order to fix the intensity, in MWatts, from the brightness temperature of the pixel affected by the fire. This expression corresponds to:

$$FRP = 4.34 \cdot 10^{-19} \left( T_{MIR}^8 - T_{MIR,b}^8 \right) \quad (6)$$

where  $T_{MIR}$  is the brightness temperature of the band of the 4  $\mu\text{m}$  of the pixel affected by the fire and  $T_{MIR,b}$  is the same temperature in the adjacent pixels. In order to carry out a validation of the results obtained at a sub-pixel level, that is, the fire's temperature and the fire's area, a comparison with the intensity values calculated through Stefan-Boltzmann's law and the previous formula has been carried out. This has been exclusively done for the MODIS sensor and on the large fires that affected Spain and Portugal during the summer of 2003. Besides, the comparison has been done for the Terra and Aqua spacecraft and at two processing levels: level of individual burning pixels and level of averaged clusters. The results of this comparison can be found in Calle *et al.* (2005), in which the two processing levels are represented separately. The almost exact coincidence of the values, which are even better in the case of the analysis at a cluster level, proves the reliability of the magnitudes temperature and area of fire. It is very important to highlight the fact that the coincidence between the empiric expression and Stefan-Boltzmann's law, after applying Dozier methodology) are coming from the analysis of clusters. However, when results are compared at the level of individual pixels, the differences are much more noticeable; so, the use of empiric expression is recommended. When sensor has a high spatial resolution in the thermal bands, the sub pixel analysis is a useful tool in order to discriminate the increasing direction of fire: that is, the flaming front. The figure 5 shows the results of the application of the sub-pixel analysis on one of the active fires that have been described. It corresponds to the superposition of the fire's temperatures on the BIRD sensor over NIR image, showing the affected fire area.

The real usefulness of remote-sensing in the early detection of fires will take place when the time resolution of the sensors implied is around 15 minutes or less. At present, this characteristic is only available in the geostationary satellites, but they have the problem of their low spatial resolution. The advantage of geostationary sensors is that it's possible to obtaining, not only the FRP but the FRE too. The fire radiative energy will be:  $FRE = \int FRP dt$ . In any case, the comparison of FRP results among sensors is only valid for qualitative purposes since in certain fires the lowest spatial resolution implies an important underestimation of this magnitude. This happens for example when comparing MSG and MODIS or MODIS and BIRD. With respect to the latter ones, Wooster *et al* (2003) found differences of up to 46%.

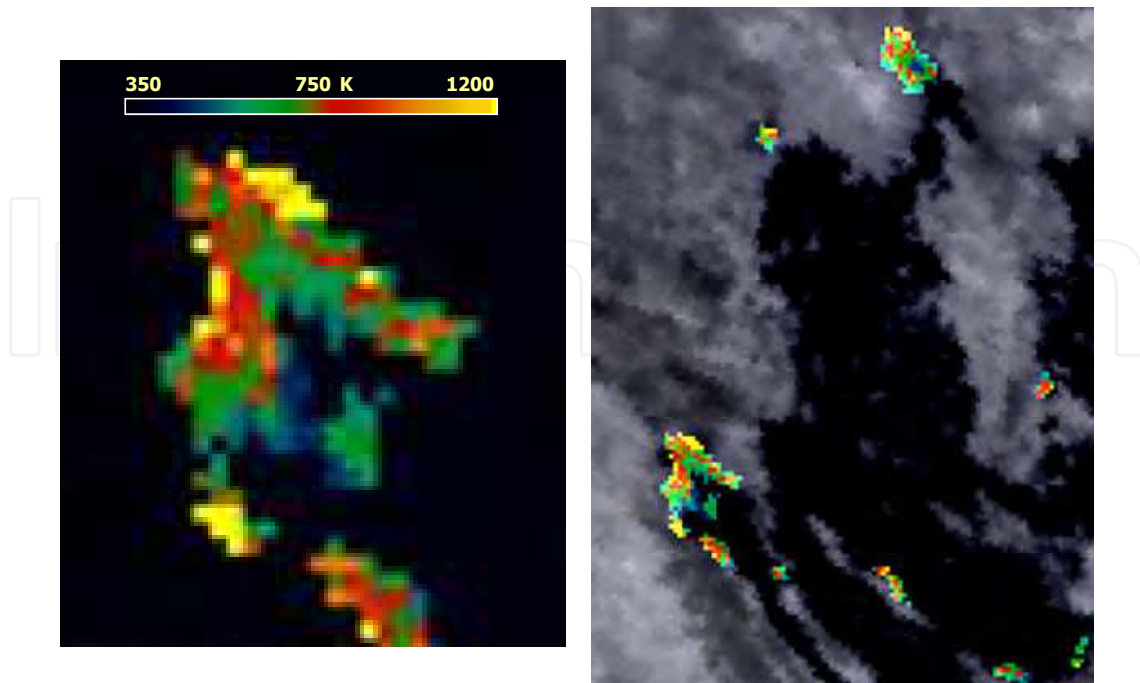


Fig. 5. This figure shows the fire temperatures, obtained by means of Dozier methodology. At this spatial resolution is very clear to recognize the flaming front and the spreading direction of fire (Calle *et al.*, 2005).

## 5. Atmospheric impact of fire emissions

The gases belonging to carbon cycle, CO and CO<sub>2</sub>, are trace gases located in the atmosphere, mostly as the result of anthropogenic activities. Despite not being a greenhouse gas, the carbon monoxide plays a significant role in the carbon cycle; it is not a direct precursor of CO<sub>2</sub>, but it essentially affects the budgets of OH radicals and O<sub>3</sub> present in the atmosphere (see Bergamaschi *et al.*, 2000, for an extended explanation about the modelling of the global CO cycle). The anthropogenic activities related to release carbon into the atmosphere can be divided in two well-defined groups: on the one hand, the urban pollutant emissions from vehicles and other industrial processes; on the other, from fires and global biomass burning emissions. The estimation of CO profiles and CO total column has been identified as a very important objective in order to improve our understanding of climate global system. The EOS (Earth Observing System) Science Steering Committee has proposed: "The fate of carbon monoxide, remotely detected from space, in conjunction with a few other critical meteorological and chemical parameters, is crucial to our understanding of the chemical reaction sequences that occur in the entire troposphere and govern most of the biogeochemical trace gases" (EOS, 1987). In the same line, the WMO (World Meteorological Organization) has proposed: "Definition of trends and distributions for troposphere CO is essential. A satellite-borne CO sensor operating for extended periods could help enormously" (WMO, 1985). The global estimation of CO based on satellite imagery involves a series of technical difficulties; the most important one is the associated error of the measurements.

The combustion by fire is a chemical reaction with heat release where the main products generated are, if combustion is completed,  $H_2O$ ,  $CO_2$ , and  $N_2$ . In the case of high combustion temperatures,  $NO_2$  and  $NO$  are released too. However it must be pointed out that the main cause of CO fire-related emissions is the incomplete or inefficient burning of wood, biomass and fossil fuels. Concerning wildfires, two phases are considered: the flaming phase (in which  $CO_2$  and nitrogen are released), and smouldering phase (in which CO and hydrocarbons are released). Two procedures provide estimations of CO emissions, a direct procedure and an indirect one. The indirect method estimates CO mass from the knowledge of the previous burned biomass. This value can be obtained from satellite cartography of fire-affected areas and the vegetation index, which is the main indicator of biomass quantity on a global scale. The adjustment of the measurements is carried out by introducing the combustion efficiency coefficients of this particular gas. This procedure was first proposed by Seiler and Crutzen (1980), who estimated CO emissions according to the following indirect parameters: i) burned land cover area ( $m^2$ ), ii) above-ground biomass density of burned area ( $kg\text{-dry-matter}/m^2$ ), iii) burning efficiency of the above-ground biomass (that is, the fraction of biomass burned) dimensionless, and iv) the emission factor ( $g$  of CO [ $kg$  dry matter] $^{-1}$ ), which varies according to the type of vegetation and ecosystem. Note that many errors arise, from this indirect procedure, due to the uncertainty in the coefficients and, especially, in the biomass estimation, which is the main quantitative parameter.

The second procedure is the direct estimate of carbon content in the atmosphere by means of remote sensing. The SCIAMACHY (SCanning Imaging Absorption SpectroMeter for Atmospheric CHartography) onboard the European satellite ENVISAT (Bovensmann *et al.*, 1999) has provided more measurements, of the most important trace gases, than any other sensor up to the present. The CO total column is retrieved from a small spectral fitting window located in SCIAMACHY channel 8 (2.324-2.335  $\mu m$ ); finally, the results of its measurements are adjusted according to the parameters of trace gas. Dils *et al.*, (2006) have carried out a series of comparisons between SCIAMACHY measurements and ground-station data. In the case of CO and  $CH_4$ , with similar algorithms, they have shown that the measurements provide good description of seasonal and latitudinal variability. However, they show important discrepancies in concrete cases. Besides, they show long periods in which the algorithm does not provide any data. The MOPITT (Measurements of Pollution in the Troposphere) instrument, onboard the Terra spacecraft, has proved to be the most operative sensor for the continuous estimation of CO. On the other hand, scientists from the NCAR (National Centre for Atmospheric Research), funded by NASA, have spread data and results concerning the global distribution of CO based on MOPITT measurements (<http://www.acd.ucar.edu/>), which have revealed the seasonal dynamics of CO throughout the planet and direct correlations between the increase in the CO total column measured by MOPITT and large fires. The validation of the results reveals the suitability of the MOPITT's spatial scale for monitoring continuously (at regional and global scale) observations of the spatial oscillations related to the atmospheric CO. Hereby, large horizontal gradients in the distribution of CO at the synoptic scale have been observed. These variations in CO can be as large as 50-100% and occur over spatial scales of around 100 km. These events, usually during several days, can span horizontal distances of 600-1000 km, and can appear over a range of pressure levels from 850 to 150 hPa (Liu *et al.*, 2006).

The biomass burning is a very important source of ozone and methane precursors and the main factor of CO emissions. High levels of carbon monoxide pollution are found around the world, and they result from different types of biomass burning in different locations. High levels of CO are linked to widespread fire activity, such as agricultural burning in central Africa in January through March, or in Central America in April through June. Carbon monoxide molecules can last from a few weeks to several months in the atmosphere, and they travel long distances, without regard for national or international boundaries. Emissions from biomass burning accounts for about one quarter of the CO released to the atmosphere, with an average of around 600 Mt CO per year (Khalil *et al.*, 1999). The occurrence of biomass burning, the size of fire, the different phases of fire considered (e.g. smouldering and flaming) and fire parameters (e.g. fire radiative power and temperature) vary greatly with time and space. Andreae and Merlet (2001) estimated that mean CO emission from vegetation fires in savanna and tropical forests is 342 Mt CO per year, while the total CO emission for all non-tropical forest fires is 68 Mt CO per year.

The pattern of fire occurrence in Africa and Amazonia is quite different to others regions in the planet with higher population density. The fire occurrence, in Africa and Amazonia, is dominated by the displacement of ITCZ (Inter Tropical Convergence Zone). During the winter of North hemisphere the ITCZ, and therefore the tropical rain, is located in the South of equator and Amazonia; so, the fire occurrence is stronger in the North of equator and vice versa. The figure 6 shows the results of seasonal study of CO in the North equatorial Africa ([4.5N-15N] and [17W-37E]), South equatorial Africa ([22S-3S] and [10E-40E]) and Amazonia ([20S-7.5S] and [65W-50W]). The bar diagram shows fire occurrence from MODIS (Giglio *et al.*, 2003; Davies *et al.*, 2009) in the period 2003-2008. In the background, in grey colour, the original data of CO total column, from MOPITT, are shown. In black colour, the inverse Fast Fourier Transform calculated by means of main harmonics with higher spectral energy. Finally, CO values from SCIAMACHY, averaged for each month, are displayed for the period 2003-2005, in order to compare results between MOPITT and SCIAMACHY sensors. Comparison between CO from MOPITT and SCIAMACHY have been carried out by Buchwitz *et al.* (2007) showing results over cities; so, this comparison over large fires, is a complementary result in order to know the spatial capabilities of these source of data.

Concerning analysis of results over Africa, northward equator, two main harmonics with maximum spectral energy, for each year, can be observed. First maximum is located in the period of January and February, showing a very good correlation with fire occurrence. The second maximum, weaker, is located in August, exactly when fire occurrence in the South of equatorial Africa is stronger. Concerning comparison between MOPITT (daily data) and SCIAMACHY CO total column is similar between them (having MOPITT data more amplitude). This is an expected difference, once SCIAMACHY data are averaged values. As we have underlined in the paragraph before, during the summer of North hemisphere the displacement of ITCZ is the responsible of a stronger fire occurrence in the South equator. Three main maximums, for each year, can be observed. The first maximum, with the shape of a peak, is located at the end of September, showing a very good correlation with the main fire occurrence in the year. The second maximum, weaker, is located at the end of January when fire occurrence in the North of equatorial Africa is stronger (see discussion before). The main difference with North equatorial Africa is the presence of a third harmonic providing an increasing tendency, of CO values, during June-September. As it's possible to

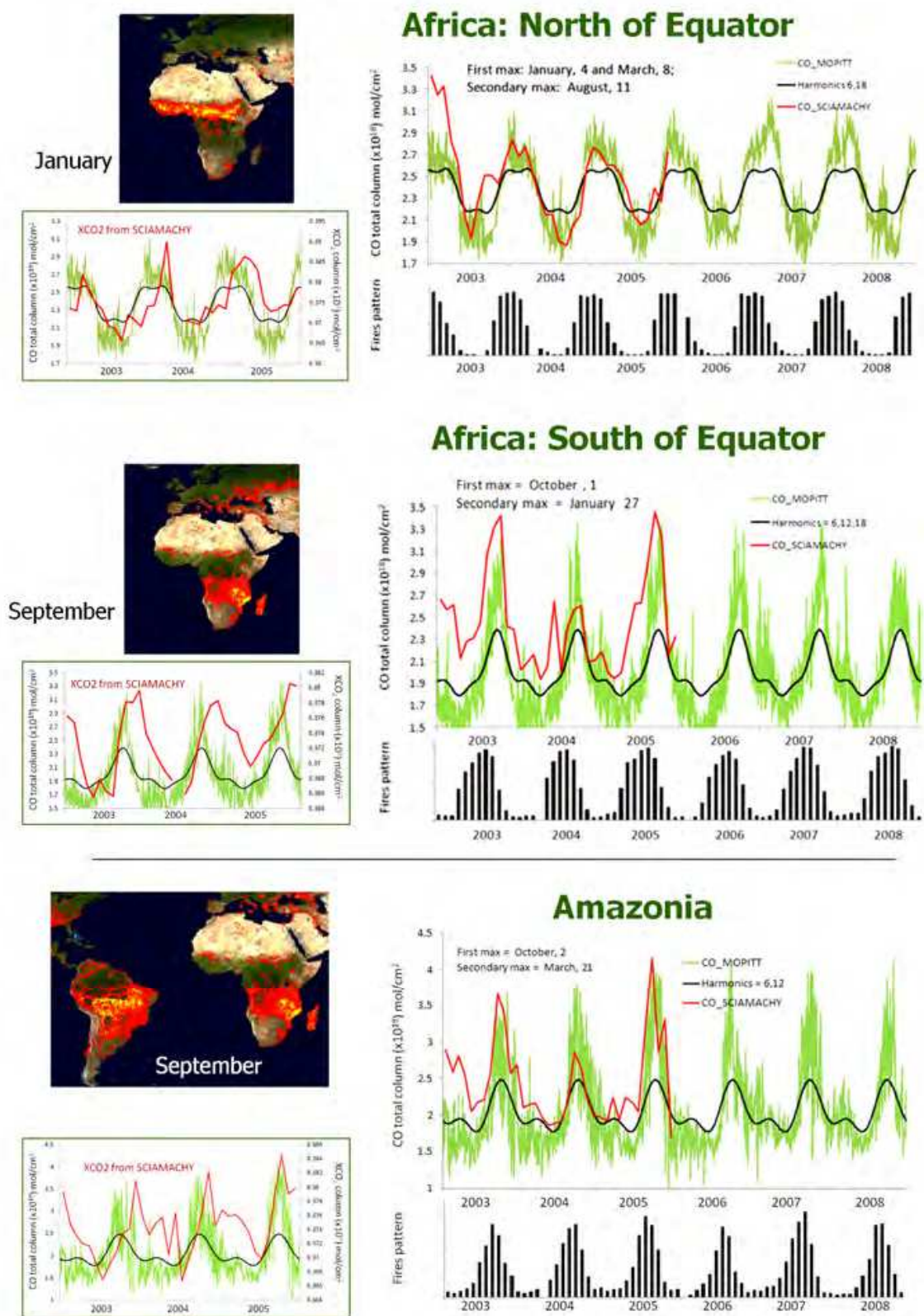


Fig. 6. Results of seasonal study of CO in Africa (North and South of equator) and Amazonia. A comparison between CO emissions and fire occurrences is shown. CO total column original values and Inverse FFT transform is underlined. Left part of each graph contains XCO<sub>2</sub> evolution for 2003-05. (Calle *et al.*, 2011).

observe in the figure 6, both geographical bands present a correlation between CO values and fire occurrence. But CO maximum values have a delay of 15-20 days with respect to maximum fire occurrence; additionally the local maximum of North band presents a coincidence with main maximum of South band; that is: influence between them due to CO transport processes in the atmosphere. In any case, the influence of North over the South is stronger. Concerning comparison between MOPITT (daily data) and SCIAMACHY CO total column is very similar between them. The pattern of fire occurrence in Amazonia is the same of the South of equatorial Africa, due to the ITCZ behaviour.

## 6. Conclusion

In the light of the results, the geostationary sensors prove to be a highly efficient tool in real-time forest fire management and monitoring. Despite not being originally designed as an Earth observation tool, but as a meteorological satellite, its excellent time resolution has proved useful for the detection of events which vary due to radiometric rather than spatial characteristics, as is the case of forest fires. On-going parameterization of fires has a strong influence on the subsequent treatment of forest regeneration. Major efforts are currently being made in the establishment of fire severity, where the main magnitude involved is the FRE in large fires for subsequently establishing intensity and include this magnitude in atmospheric emission models. This correlation between FRE and severity was not possible with polar sensors due to their lack of continuous observation. Another important magnitude that can be established from the FRE is the height of the flame, including some characteristics of the fuel, which could help the analysis of the fire front and other magnitudes linked to its advance. This is an essential magnitude since it is used by fire fighting services to determine the infrastructure necessary to combat fires. Both, the EOS Science Steering Committee and the WMO, have pointed out, as a main objective, the measurement and control of carbon monoxide as part of the control framework of trace gases involved in the carbon cycle. Forest fires are an important source of CO and CO<sub>2</sub> worldwide. However, the global estimates carried out have been based on indirect methods which require the previous determination of the burned areas and the introduction of burning efficiency coefficients, which are difficult to determine. In order to apply direct methods for emissions estimating, atmospheric sensors as MOPITT and SCIAMACHY have proven their ability to extract important conclusions about carbon cycle gases at global scale.

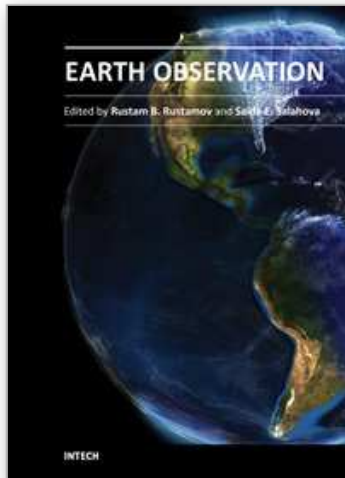
## 7. References

- Al-Rawi, K-L-, Casanova, J.L. & Calle, A. (2001). Burned area mapping system and fire detection system, based on neural networks and NOAA-AVHRR imagery. *International Journal of Remote Sensing*, 22, 2015-2032. ISSN: 0143-1161
- Andreae, M. O. and Merlet, P. (2001). Emission of trace gases and aerosols from biomass burning. *Global Biogeochemical Cycles*, 15:955-966. ISSN: 0886-6236
- Arino, O. and Rosaz, J.M. (1999), 1997 and 1998 World ATSR FIRE Atlas using ERS-2 ATSR-2 Data, *Proceedings of the Joint Fire Science Conference*, Boise, 15-17, June 1999.
- Arino, O., and Mellinotte, J.M. (1998). The 1993 Africa fire map, *International Journal of Remote Sensing*, 19:2019-2023. ISSN: 0143-1161

- Bergamaschi, P., Hein, R., Heimann, M. and Crutzen, P. J. (2000): Inverse modelling of the global CO cycle, 1. Inversion of CO mixing ratios. *Journal of Geophysical Research*, 105:1909–1927. ISSN: 0148-0227
- Berk, A., Bernstein, L.W. and Robertson, D.C. (1996), MODTRAN: A moderate resolution model for LOWTRAN 7, Philips Laboratory, Report AFGL-TR-83-0187, Hanscom ARB, MA.
- Bovensmann, H., Burrows, J. P., Buchwitz, M., Frerick, J., Noël, S., Rozanov, V. V., Chance, K. V. and Goede, A. (1999). SCIAMACHY- Mission Objectives and Measurement Modes. *Journal of Atmospheric Sciences*, 56:127–150. ISSN 0022-4928
- Briess, K., Jahn, H., Lorenz, E., Oertel, D., Skrbek, W. & Zhukov, B. (2003). Fire recognition potential of the bi-spectral detection (BIRD) satellite. *International Journal of Remote Sensing*, 24, 865-872. ISSN: 0143-1161
- Buchwitz, M., Khlystova, I., Bovensmann, H., and Burrows, J.P. (2007). Three years of global carbon monoxide from SCIAMACHY: comparison with MOPITT and first results related to the detection of enhanced CO over cities. *Atmospheric Chemistry and Physics*, 7:2399–2411. ISSN: 1680-7316
- Calle, A., Romo, A., Sanz, J. & Casanova, J.L. (2005). Analysis of forest fire parameters using BIRD, MODIS and MSG-SEVIRI sensors. *New Strategies for European Remote Sensing*, Millpress, Rotterdam, ISBN 90 5966 003.
- Calle, A., Casanova, J.L. and Romo, A. (2006). Fire detection and monitoring using MSG Spinning Enhanced Visible and Infrared Imager (SEVIRI) data. *Journal of Geophysical Research*, 111, G04S06, doi:10.1029/2005JG000116.
- Calle, A., Casanova, J.L. and Romo, A. (2009). Impact of point spread function of MSG-SEVIRI on active fire detection. *International Journal of Remote Sensing*, 30(17), 4567–4579. ISSN: 0143-1161
- Calle, A., Salvador, P. and González, F. (2011). Study of the impact of wildfires emissions, through MOPITT CO total column, at different spatial scales. *International Journal of Remote Sensing* (in press). ISSN: 0143-1161
- Casanova, J.L., Calle, A. and González-Alonso F. (1998). A Forest Fire Risk Assessment obtained in real time by means of NOAA satellite images. *Forest Fire Research. III. International Conference on Forest Fire Research and 14<sup>th</sup> Conference on Fire and Forest Meteorology*. Vol I: 1169-1179. ISBN: 972-97973-0-7
- Chuvieco, E., Riaño, D., Aguado, I. and Cocero, D. (2002). Estimation of fuel moisture content from multitemporal analysis of Landsat Thematic Mapper reflectance data: applications in fire danger assessment. *International Journal of Remote Sensing*, 23 (11):2145-2162. ISSN: 0143-1161
- Cracknell, A.P. (1998). Review article synergy in remote sensing-what's in a pixel? *International Journal of Remote Sensing*, 19, 2025-2047. ISSN: 0143-1161
- Davies, D.K., Ilavajhala, S., Wong, M.M., and Justice, C.O. (2009). Fire Information for Resource Management System: Archiving and Distributing MODIS Active Fire Data. *IEEE Trans. on Geoscience and Remote Sensing*, 47 (1):72-79. ISSN: 0196-2892
- Dils, B., et al. (2006). Comparisons between SCIAMACHY and ground-based FTIR data for total columns of CO, CH<sub>4</sub>, CO<sub>2</sub> and N<sub>2</sub>O. *Atmospheric Chemistry and Physics*, 6:1953–1976. ISSN: 1680-7316
- Dozier, J. (1981). A method for satellite identification of surface temperature fields of subpixel resolution. *Remote Sensing of Environment*, 11: 221-229. ISSN: 0034-4257

- Giglio, L. & Kendall, J.D., (2001). Application of the Dozier retrieval to wildfire characterization. A sensitivity analysis. *Remote Sensing of Environment*, 77, 34-49. ISSN: 0034-4257
- Giglio, L. & Justice, C.O. (2003). Effect of wavelength selection on characterisation of fire size and temperature. *Int. Journal of Remote Sensing*, 24,3515-3520. ISSN:0143-1161
- Giglio, L., Descloitres, J., Justice, C.O. & Kaufman, Y.J. (2003). An enhanced contextual fire detection algorithm for MODIS. *Remote Sensing of Environment*, 87:273-282. ISSN: 0034-4257
- Hunt, E.R. & Rock, C.R. (1989). Detection of changes in leaf water content using near and medium infrared reflectances. *Remote Sensing of Env.*, 30:43-54. ISSN:0034-4257
- Ichoku, C., Kaufman, Y.J., Giglio, L., Li, Z., Fraser, R.H., Jin, J-Z & Park, W.M. (2003). Comparative analysis of daytime fire detection algorithms using AVHRR data for the 1995 fire season in Canada: perspective for MODIS. *International Journal of Remote Sensing*, 24, 1669-1690. ISSN: 0143-1161
- Illera, P. Fernández, A., Calle, A. and Casanova, J.L. (1996). Evaluation of fire danger in Spain by means of NOAA-AVHRR images. *EARSeL Journal Advance in Remote Sensing*, 4-4:33-43. ISSN: 1017-4613
- Justice, C.O & Malingreau, J.P.(editors). (1993). The IGBP satellite fire detection algorithm workshop technical report, IGBP-DIS Working paper 9, NASA/GSFC, Greenbelt, Maryland, USA, February, 1993.
- Khalil, M. A. K, Pinto, J. P. and Shearer, M. J. (1999). Atmospheric carbon monoxide. *Chemosphere: Global Change Science*, 1, IX -XI. ISSN: 1465-9972
- Kaufman, Y. & Justice, C. (1998). MODIS Fire Products. MODIS Science Team. EOS ID#2741
- Kaufman, Y.J., Justice, C., Flynn, L. Kendall, J. Prins, E., Ward, D.E., Menzel, P. & Setzer, A. (1998). Potencial global fire monitoring from EOS-MODIS. *Journal of Geophysical Research*, 103, 32215-32238. ISSN: 0148-0227
- Langaas, S. (1995). A critical review of sub-resolution fire detection techniques and principles using thermal satellite data. *PhD thesis*, Department of Geography, University of Oslo, Norway.
- Lasaponara, R. Cuomo, V. and Tramutoli, V. (1998). Satellite forest fire detection in the Italian ecosystems using AVHRR data. *XII Int. Conference on Forest Fire Research Luso* 16/20 nov. 1998, vol II, 2013-2028
- Li, Z., Nadon, S., Chilar, J. & Stocks, B. (2000). Satellite mapping of Canadian boreal forest fires: Evaluation and comparison of algorithms. *International Journal of Remote Sensing*, 21, 3071-3082. ISSN: 0143-1161
- Li, Z., Kaufman, Y.J., Ichoku, C, Fraser, R., Trishchenko, A., Giglio, L. Jin, J and Yu, X. (2001). A review of AVHRR-based active fire detection algorithms: Principles, limitations and recommendations in Global and Regional vegetation fire monitoring from space: Planning a coordinated international effort, SPB Academic Publishing, The Hague, Netherlands, pp. 199-225.
- Liu, J., Drummond, J.R., Jones, D.B.A., Cao, Z., Bremer, H. Kar, J. Zou, J., Nichitiu, F. and Gille, J.C. (2006). Large horizontal gradients in atmospheric CO at the synoptic scale as seen by spaceborne Measurements of Pollution in the Troposphere. *Journal of Geophysical Research*, 111, D02306, doi:10.1029/2005JD006076.

- Matson, M. and Dozier, J. (1981). Identification of sub-resolution high temperatures sources using a thermal IR sensor. *Photogrammetric Engineering and Remote Sensing*, 47(9), 1311-1318. ISSN: 0099-1112
- Nemani, R.R. and Running, S.W., (1989). Estimation of regional surface resistance to evapotranspiration from NDVI and thermal IR AVHRR data. *Journal of Applied Meteorology*, 28 (4): 276-274. ISSN: 0894-8763
- Price, J. C. 1984, Land surface temperature measurements from the split window channels of the NOAA 7 AVHRR, *Journal of Geophysical Research*. D5:7231-7237. ISSN: 0148-0227
- Prins, E.M. and Menzel, W.P. 1994. Trends in South American burning detected with the GOES VAS from 1983-1991. *Journal of Geophysical Research*, 99 (D8), 16719-16735. ISSN: 0148-0227
- Prins, E., Govaerts, Y. and Justice, C.O. (2004), Report on the Joint GOFD/GOLD Fire and CEOS LPV Working Group Workshop on Global Geostationary Fire Monitoring Applications, GOFD/GOLD Report No. 19. 23-25 March 2004. EUMETSAT, Darmstadt, Germany.
- Robinson, J.M., (1991). Fire from space: Global fire evaluation using infrared remote sensing. *International Journal of Remote Sensing*, 12: 3-24. ISSN: 0143-1161
- Roldán-Zamarrón, A., S. Merino-de-Miguel, F. González-Alonso, S. García-Gigorro, and J. M. Cuevas (2006), Minas de Riotinto (south Spain) forest fire: Burned area assessment and fire severity mapping using Landsat 5-TM, Envisat-MERIS, and Terra-MODIS postfire images, *Journal of Geophysical Research*, 111, G04S11, doi:10.1029/2005JG000136.
- Seiler, W. and Crutzen, P. J. (1980). Estimates of gross and net fluxes of carbon between the biosphere and the atmosphere from biomass burning. *Climate Change*, 2:207- 247. ISSN:0165-0009
- Wooster, M.J., Zhukov, B & Oertel, D. (2003). Fire radiative energy for quantitative study of biomass burning: derivation from the BIRD experimental satellite and comparison to MODIS fire products. *Remote Sensing of Environment*, 86, 83-107. ISSN: 0034-4257
- Wooster, M.J., Roberts, G., Perry, G.L.W and Kaufman, Y.J (2005). Retrieval of biomass combustion rates and totals from fire radiative power observations: FRP derivation and calibration relationships between biomass consumption and fire radiative energy release. *Journal of Geophysical Research*, 110, D24311, doi: 10.1029/2005JD006318



## **Earth Observation**

Edited by Dr. Rustam Rustamov

ISBN 978-953-307-973-8

Hard cover, 254 pages

**Publisher** InTech

**Published online** 27, January, 2012

**Published in print edition** January, 2012

Today, space technology is used as an excellent instrument for Earth observation applications. Data is collected using satellites and other available platforms for remote sensing. Remote sensing data collection detects a wide range of electromagnetic energy which is emitting, transmitting, or reflecting from the Earth's surface. Appropriate detection systems are needed to implement further data processing. Space technology has been found to be a successful application for studying climate change, as current and past data can be dynamically compared. This book presents different aspects of climate change and discusses space technology applications.

### **How to reference**

In order to correctly reference this scholarly work, feel free to copy and paste the following:

Abel Calle and José Luis Casanova (2012). Forest Fires and Remote Sensing, Earth Observation, Dr. Rustam Rustamov (Ed.), ISBN: 978-953-307-973-8, InTech, Available from: <http://www.intechopen.com/books/earth-observation/forest-fires-and-remote-sensing>

**INTECH**  
open science | open minds

#### **InTech Europe**

University Campus STeP Ri  
Slavka Krautzeka 83/A  
51000 Rijeka, Croatia  
Phone: +385 (51) 770 447  
Fax: +385 (51) 686 166  
[www.intechopen.com](http://www.intechopen.com)

#### **InTech China**

Unit 405, Office Block, Hotel Equatorial Shanghai  
No.65, Yan An Road (West), Shanghai, 200040, China  
中国上海市延安西路65号上海国际贵都大饭店办公楼405单元  
Phone: +86-21-62489820  
Fax: +86-21-62489821

© 2012 The Author(s). Licensee IntechOpen. This is an open access article distributed under the terms of the [Creative Commons Attribution 3.0 License](#), which permits unrestricted use, distribution, and reproduction in any medium, provided the original work is properly cited.

IntechOpen

IntechOpen